Energy Advances

ROYAL SOCIETY OF CHEMISTRY

PAPER

View Article Online
View Journal

Cite this: DOI: 10.1039/d5ya00361j

Sodium tetraphenylborate: a fluorine-free electrolyte salt for sodium-ion batteries

Darren M. C. Ould, *[ab] James M. Courtney,[a] Kyle G. Pearce,[c] Daniel J. Curtis,[a] Marcin W. Orzech,[a] Sajad Kiani,[a] Brent de Boode[d] and Serena Margadonna *[a]

Received 11th December 2025,
Accepted 1st May 2026

DOI: 10.1039/d5ya00361j

rsc.li/energy-advances

Sodium-ion batteries are a promising emerging technology due to the low cost and wide abundance of sodium, but commonly use fluorine-containing electrolyte salts, such as sodium hexafluorophosphate ($NaPF_6$), which pose safety and toxicity concerns (*e.g.* HF formation). This work investigates using sodium tetraphenylborate ($NaBPh_4$) as a non-fluorinated electrolyte salt for sodium-ion batteries. Multinuclear NMR spectroscopy studies revealed $NaBPh_4$ has excellent stability towards atmospheric air and thermogravimetric analysis (TGA) showed this salt has good thermal stability, providing convenient handling, transport and storage. Bulk conductivity measurements using $NaBPh_4$ in ethylene carbonate: diethyl carbonate (EC:DEC 1 : 1 v/v) at different concentrations found 0.5 M $NaBPh_4$ gave the highest conductivity. Battery cycling in coin cells using a Prussian white ($Na_2Fe[Fe(CN)_6]$) cathode and hard carbon anode with an upper cut-off voltage of 3.6 V showed poor capacity retention, however, lowering the upper voltage limit to 3.0 V gave stable cycling, albeit at lower capacity. Solution-state NMR spectroscopy studies on the post-cycled electrolyte found degradation of $NaBPh_4$ occurs during cycling, with triphenylborane and biphenyl hypothesised as likely electrochemical oxidation products.

Introduction

The required transition to net-zero economies requires sustainable, safe and practical energy solutions. Lithium-ion batteries (LIBs) lead the way in rechargeable battery technology, but the relative low abundance and uneven distribution of lithium deposits, along with limitations of the transition metals used in their cathode construction (commonly nickel and cobalt), means that alternative battery technologies are urgently required.[1–3] Sodium-ion batteries (SIBs) are a promising alternative technology that improves upon the sustainability of LIBs, as cobalt-free cathodes can be used and aluminium can be employed as the current collector for both anode and cathode.[4]

Appropriated from LIBs, sodium hexafluorophosphate ($NaPF_6$) is the benchmark electrolyte salt for SIBs.[5,6] This is on account of $NaPF_6$ offering the best compromise between ionic conductivity, thermal stability, electrochemical stability, safety and cost.[5] Nevertheless, the PF_6^- anion is susceptible to hydrolysis and decomposes to form hazardous HF and POF_3.[7,8] The generation of these gases is problematic as they cause degradation to cell components and add challenges for battery recycling. The presence of fluorine in the electrolyte causes wider safety concerns as in the event of cell failure, toxic gases may be released.[9,10]

Alternative electrolyte salts are available for SIBs, but the majority include fluorinated anions.[11] Sodium bis(fluorosulfonyl)imide (NaFSI) and sodium bis(trifluoromethylsulfonyl)imide (NaTFSI) are alternative electrolyte salt choices and are commonly used with ionic liquid solvents.[12,13] Although these salts are less prone to form HF than using $NaPF_6$, HF generation may still occur.[14] Moreover, NaFSI and NaTFSI salts in carbonate solvents are known to cause anodic dissolution of aluminium (commonly referred to as aluminium corrosion).[15,16]

Sodium perchlorate ($NaClO_4$) is another common electrolyte salt that is widely reported. It is a non-fluorinated salt, though the strong oxidising properties of the perchlorate anion causes safety concerns which prevents industrial application. In addition, $NaClO_4$ is reported to exhibit high water content (>40 ppm), even after drying under vacuum overnight.[11]

It would be desirable to use a non-fluorinated electrolyte salt for SIBs to alleviate safety and toxicity concerns in the electrolyte (*e.g.* HF).[17,18] However, replacing $NaPF_6$ with a non-fluorinated electrolyte salt remains challenging due to the favourable properties of a fluorinated anion. The role of fluorine has previously been investigated by comparing the

[a] Department of Chemical Engineering, Faculty of Science and Engineering, Swansea University, Swansea SA1 8EN, UK. E-mail: s.margadonna@swansea.ac.uk
[b] The Faraday Institution, Quad One, Harwell Science and Innovation Campus, Didcot, OX11 ORA, UK
[c] Department of Chemistry, University of Bath, Claverton Down, Bath, BA2 7AY, UK
[d] Batri Ltd, Unit 6a Bridgend Business Centre, Bennett Street, Bridgend, CF31 3SH, UK

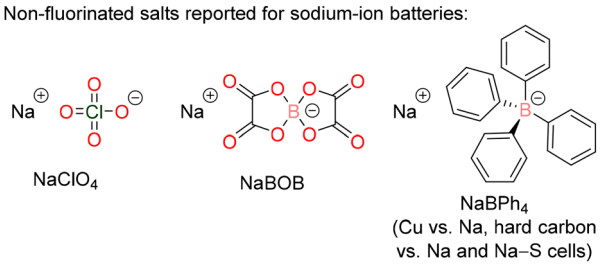

Fig. 1 Examples of non-fluorinated electrolyte salts reported for use in SIBs.

fluorinated sodium borate salt Na[B(hfip)$_4$]·DME [(hfip = OCH(CF$_3$)$_2$ (O^{i}Pr^F), DME = 1,2-dimethoxyethane] with its non-fluorinated analogue, Na[B(O^{i}Pr)$_4$] [O^{i}Pr = OCH(CH$_3$)$_2$]. Na[B(hfip)$_4$]·DME was found to have better solubility in carbonate solvents, a wider electrochemical stability window and less ion-pairing.[19]

Importantly, the presence of fluorinated species, such as NaF (formed from the decomposition of NaPF$_6$), in the solid–electrolyte interphase (SEI) are reported to be crucial to enable stable long-term cycling. It has been shown that an SEI with a low NaF content leads to inferior battery cycling.[20]

Although limited, non-fluorinated electrolyte salts have been reported for SIBs (Fig. 1). Sodium bis(oxalato)borate, Na[BOB] [BOB = bis(oxalato)borate], has been used with trimethyl phosphate (TMP), triethyl phosphate (TEP), *N*-methyl-2-pyrrolidone (NMP), or mixtures of these solvents in cells containing a Prussian white cathode (Na$_2$Fe[Fe(CN)$_6$]) and hard carbon anode.[21–23] X-ray photoelectron spectroscopy (XPS) measurements on the post-cycled hard carbon using 0.5 M Na[BOB] in TMP solvent revealed that Na[BOB], as well as TMP, contribute to the SEI.[21] Nevertheless, Na[BOB] has a low solubility in traditionally used carbonate solvents.

An alternative non-fluorinated electrolyte salt previously reported for SIBs is sodium tetraphenylborate (NaBPh$_4$, Ph = C$_6$H$_5$). 0.1 M NaBPh$_4$ in DME solvent has been used as the electrolyte in copper *vs.* sodium cells, where stable sodium plating and stripping at an average of 99.85% Coulombic efficiency over 300 cycles was reported.[24] This electrolyte showed high initial Coulombic efficiency and low polarisation, with negligible increase in polarisation over 100 cycles. This is in contrast to the low initial Coulombic efficiency and large polarisation observed when using 1 M NaPF$_6$ in ethylene carbonate: diethyl carbonate (EC:DEC) as the electrolyte. Interfacial studies using XPS on the formed SEI found a thin SEI that was predominantly composed of carbon, oxygen and sodium. Moreover, the reduction products of DME, *e.g.* alkoxides, were found and there were negligible quantities of boron-based compounds. The low amounts of boron present in the SEI likely means there was little/no decomposition of the [BPh$_4$]$^-$ anion on sodium metal.[24]

Reversible charge/discharge cycling in hard carbon *vs.* sodium half cells has been reported using 0.5 M NaBPh$_4$ in DME as the electrolyte, giving highly stable charge/discharge cycling.[25] The stable cycling was in part explained by the low polarisation which was observed in these cells, with lower polarisation than using 1 M NaPF$_6$ in EC:DEC. Interfacial studies using XPS on the hard carbon again found negligible quantities of boron-based species and instead found a thin SEI that was derived from DME.[25] A separate study has used 0.1 M NaBPh$_4$ in DME as the electrolyte for application in a Na–S battery, using a Sn anode and sulfurized polyacrylonitrile (SPAN) as the cathode.[26] This gave a specific capacity greater than 200 mAh g^{-1} for 40 cycles at room temperature.[26] Lastly, the solution structure of NaBPh$_4$ has been studied in different organic solvents.[27] It was found that short-range stacking between [BPh$_4$]$^-$ anions exists when using concentrated solutions of NaBPh$_4$ in propylene carbonate (PC), forming clusters with the solvated Na$^+$ cations. In the other solvents studied (DME, acetonitrile and tetrahydrofuran), these clusters were rarely seen.[27] Despite these reported examples, NaBPh$_4$ has not been studied in sodium-ion full-cells using a Prussian white cathode and hard carbon anode.

This work investigates the electrochemical properties and application of NaBPh$_4$ as a non-fluorinated electrolyte salt for SIBs in full-cells employing a Prussian white cathode and hard carbon anode. The NaBPh$_4$ salt was found to possess excellent stability to atmospheric air and has good thermal stability. Bulk conductivity measurements found 0.5 M NaBPh$_4$ in EC:DEC (1 : 1 v/v) solvent gave the highest conductivity of the concentrations studied. This concentration was used as the electrolyte for full-cell cycling, where stable cycling was observed using voltage limits of 1.5–3.0 V.

Results and discussion

The thermal properties of sodium tetraphenylborate (NaBPh$_4$) were investigated by using thermogravimetric analysis (TGA). From the TGA profile (Fig. 2), NaBPh$_4$ showed a major decomposition step beginning at approximately 226 °C (1st derivative temperature 288 °C, Fig. S1), with a secondary process occurring with a 1st derivative temperature of 357 °C. This accounts

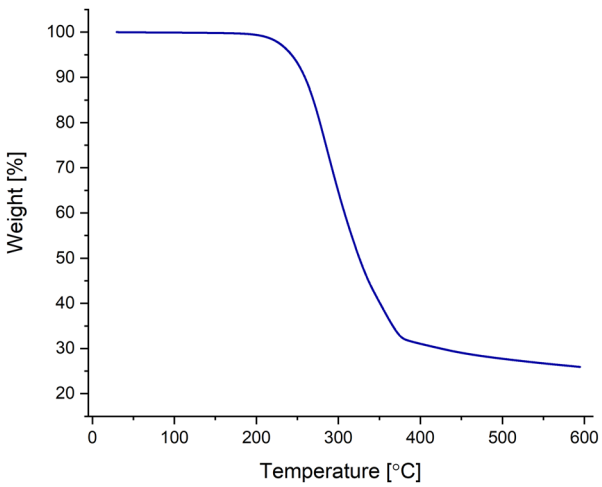

Fig. 2 TGA curve for NaBPh$_4$ under an argon flow with a heating rate of 10 °C min^{-1}.

for the majority mass loss (67%). A further minor decomposition step then occurs at approximately 374 °C and the TGA trace continues to lose weight until the end temperature at 600 °C. The weight loss associated with this step is small (7%). The total weight loss during the TGA experiment was 74%. Previously, it was reported that $NaBPh_4$ thermally decomposes to $NaBO_2$ in air.[28]

The atmospheric air stability of $NaBPh_4$ was then determined. An electrolyte salt that is stable to air is advantageous as this allows for safe and convenient handling, transport and storage. For this, 0.1 mmol of $NaBPh_4$ was left exposed to air in an uncapped vial at room temperature for 1 month (30 days). Solution-state multinuclear NMR spectroscopy of the air exposed salt in DMSO-d_6 solvent was then recorded. After 1 month, ^{1}H NMR and ^{11}B NMR spectra revealed no degradation of the salt had occurred, with the ^{1}H NMR spectrum showing the expected three aromatic signals (δ_H = 7.27, 7.00 and 6.86 ppm) and the ^{11}B NMR showing retention of the singlet at δ_B = −6.6 ppm (Fig. 3). Thus, $NaBPh_4$ exhibits high stability towards atmospheric air.

While 1 M $NaPF_6$ in carbonate solvent(s) is commonly used as the electrolyte for SIBs,[6] for $NaBPh_4$, bulk conductivity measurements were performed to determine which electrolyte concentration to proceed with. The electrolyte concentrations tested were 0.1 M, 0.25 M, 0.5 M, 1.0 M and 1.5 M $NaBPh_4$ in ethylene carbonate: diethyl carbonate (EC:DEC 1 : 1 v/v), which gave a range of low to high concentrations.

As shown in Fig. 4, the bulk conductivities (measured at 25 °C using electrochemical impedance spectroscopy) initially increase with increasing electrolyte concentration, reaching a maximum for 0.5 M $NaBPh_4$ (3.6 mS cm^{-1}). The conductivity values for the 0.1 M and 0.25 M $NaBPh_4$ electrolytes are 1.9 mS cm^{-1} and 2.9 mS cm^{-1}, respectively. Beyond 0.5 M, the conductivity of $NaBPh_4$ in EC:DEC began to sharply decrease, with the 1 M $NaBPh_4$ and 1.5 M $NaBPh_4$ electrolytes giving bulk conductivity values of 2.6 mS cm^{-1} and 1.6 mS cm^{-1}, respectively. For comparison, 0.5 M $NaPF_6$ and 1 M $NaPF_6$ in EC:DEC (1 : 1 v/v) solvents have reported bulk conductivities of 7.4 mS cm^{-1} and 8.8 mS mS cm^{-1}, respectively.[6] Although these values are higher than for 0.5 M $NaBPh_4$ in EC:DEC, the bulk conductivity of 0.5 M $NaBPh_4$ is the same order of magnitude.

To explain the bulk conductivity results, the dynamic viscosities and self-diffusion coefficients (D) of the different electrolyte solutions were determined. The viscosity of the electrolyte is a crucial property as a highly viscous electrolyte will hinder ion mobility. Moreover, the viscosity can affect the wetting of the electrodes and separator in the battery.

For the $NaBPh_4$ solutions, the dynamic viscosities increased with increasing salt concentration (Fig. 4 and Table S1). The neat EC:DEC (1 : 1 v/v) solvent has a viscosity of 1.48 cP. A small increase in viscosity was seen for the 0.1 M $NaBPh_4$ electrolyte (1.76 cP) and the viscosity further increased for the 0.25 M and 0.5 M $NaBPh_4$ electrolytes, 2.22 and 3.67 cP, respectively. For the 1 M and 1.5 M $NaBPh_4$ solutions, large increases in dynamic viscosity were observed, measuring 10.10 cP and

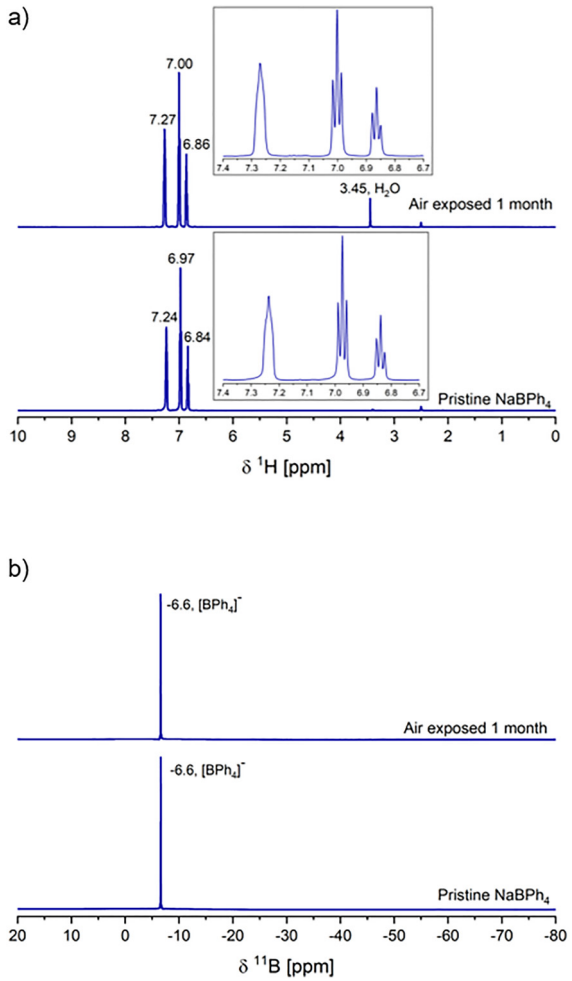

Fig. 3 (a) ^{1}H NMR (500 MHz, $(CD_3)_2SO$, 295 K) and (b) ^{11}B NMR (160 MHz, $(CD_3)_2SO$, 295 K) spectra of the soluble products after leaving 0.1 mmol of $NaBPh_4$ exposed to atmospheric air in an uncapped vial at room temperature for 1 month (30 days). Inserts show the aromatic region (7.40–6.70 ppm) of the ^{1}H NMR spectrum.

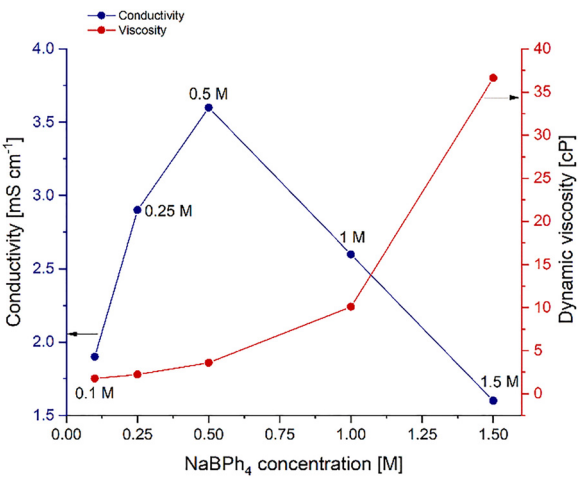

Fig. 4 Bulk conductivity (blue) and dynamic viscosity values (red) of 0.1 M, 0.25 M, 0.5 M, 1 M, and 1.5 M $NaBPh_4$ in EC:DEC (1 : 1 v/v) electrolytes at 25 °C.

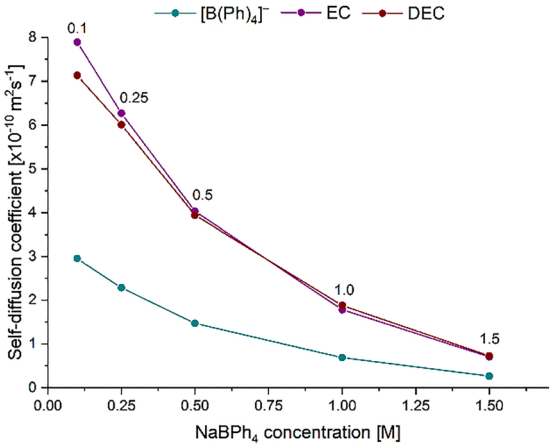

Fig. 5 Self-diffusion coefficients (D) of the $[BPh_4]^-$ anion (green), EC solvent (purple) and DEC (CH_3 group, red) solvent using ^{1}H DOSY NMR. Electrolytes are 0.1 M, 0.25 M, 0.5 M, 1.0 M and 1.5 M $NaBPh_4$ in EC:DEC (1:1 v/v).

36.62 cP, respectively. The reason for 0.5 M $NaBPh_4$ possessing the highest bulk conductivity can therefore be seen as a balance between the increase in the number of conductive charge carriers in solution *versus* the corresponding large increase in the solution viscosity beyond 0.5 M concentration.

The self-diffusion coefficients of the solvent ($D_{solvent}$) and $[BPh_4]^-$ anion (D_{anion}) were determined using ^{1}H NMR diffusion-ordered spectroscopy (DOSY) (Fig. 5 and Table S2). The relationship between the D and viscosity is given by the Stokes–Einstein equation, which states for spherical, non-interacting particles, D should be inversely proportional to viscosity. Other factors may also influence the D with changing concentration, including changes to the solvation shells of ions and ion–ion interactions.

For the $[BPh_4]^-$ anion, the D_{anion} decreased with increasing salt concentration. This is explained by the corresponding increase in solution viscosity and the likely increase in ion-pairing interactions and possible aggregate formation. Accordingly, the $D_{solvent}$ of both EC and DEC molecules decreased with increasing salt concentration, where the values of $D_{solvent}$ were approximately the same for both EC and DEC.

The $D_{solvent}$ values were higher than for the D_{anion} values at all electrolyte concentrations. Neutral solvent molecules are expected to experience less resistance moving through the solution than charged ions, especially those that are not coordinated to Na^+ cations. The difference between the $D_{solvent}$ and D_{anion} values was greatest for the 0.1 M $NaBPh_4$ electrolyte and least for 1.5 M $NaBPh_4$. This correlates with a decrease in the number of available solvent molecules (*i.e.* not coordinated to Na^+) with increasing salt concentration, assuming the coordination shell of Na^+ remains constant across all electrolyte concentrations (see SI).

The electrochemical stability window (ESW) of $NaBPh_4$ in EC:DEC was studied using cyclic voltammetry (CV). CV measurements were performed in a three-electrode cell with glassy carbon and aluminium foil as the working electrodes; platinum was used as the counter electrode and sodium metal was the pseudo-reference. As the 0.5 M $NaBPh_4$ in EC:DEC (1:1 v/v) electrolyte gave the highest bulk conductivity, it was chosen as the electrolyte to proceed with. For comparison, the ESW of the higher electrolyte concentrations 1 M $NaBPh_4$ and 1.5 M $NaBPh_4$ in EC:DEC were also studied. In all CV experiments, the current density decreased with increasing cycle number (*e.g.* see Fig. S4).

When using glassy carbon as the working electrode, 0.5 M $NaBPh_4$ had an ESW between 1.4–3.2 V *vs.* Na/Na^+, as determined from the 2nd cycle at a scan rate of 10 mV s^{-1}. Beyond this voltage window, the current densities began to significantly increase, especially on the anodic sweep (Fig. 6a).

CV measurements were recorded using aluminium foil as the working electrode as it is commonly used as the current collector in SIBs (Fig. 6b). For the 0.5 M $NaBPh_4$ in EC:DEC

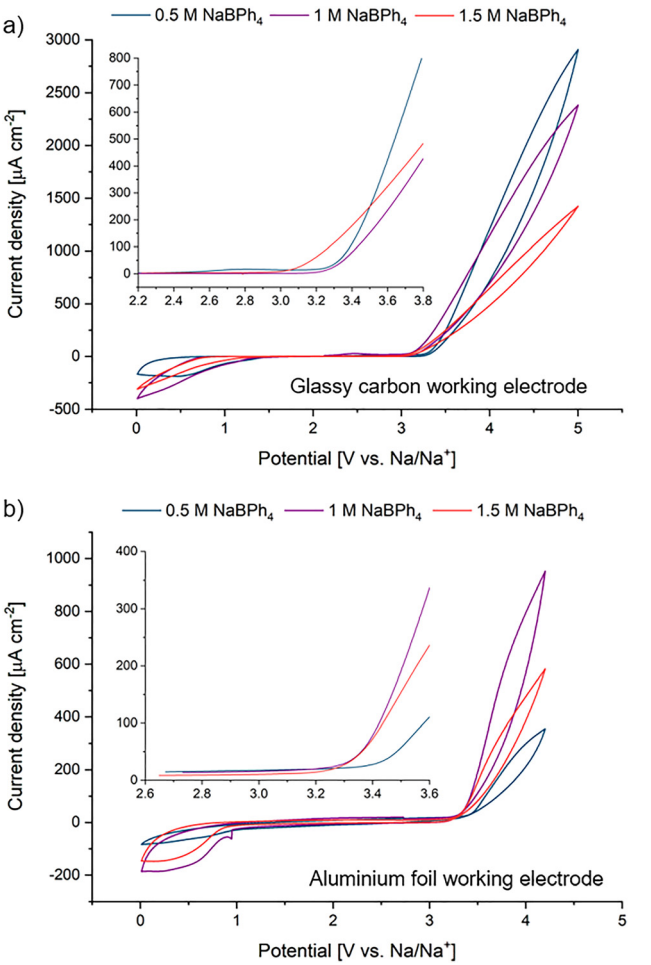

Fig. 6 Cyclic voltammetry of 0.5 M $NaBPh_4$ (blue), 1 M $NaBPh_4$ (purple) and 1.5 M $NaBPh_4$ (red) in EC:DEC (1:1 v/v) in three-electrode cell. (a) Working electrode: glassy carbon, counter electrode: platinum and reference electrode: sodium metal. Measured between 0.01–5.0 V *vs.* Na/Na^+ at 10 mV s^{-1}. (b) Working electrode: aluminium foil, counter electrode: platinum and reference electrode: sodium metal. Measured between 0.01–4.2 V *vs.* Na/Na^+ at 5 mV s^{-1}. 2nd cycle shown.

(1:1 v/v) electrolyte, it was oxidatively stable up to 3.4 V *vs.* Na/Na^+, after which the current densities significantly increased. The crossover of forward (oxidative) and reverse (reductive) scans observed when using the $NaBPh_4$-containing electrolytes indicate a complex interface at these potentials on aluminium surfaces (Fig. S7–S9). Nevertheless, scanning electron microscopy (SEM) images of the post-cycled aluminium foils did not reveal pitting or signs of degraded aluminium (Fig. S10).

Extended charge/discharge cycling was performed to investigate the suitability of using $NaBPh_4$ as a non-fluorinated electrolyte salt. Coin cells were constructed using 0.5 M $NaBPh_4$ in EC:DEC (1:1 v/v) solvent as the electrolyte. A Prussian white cathode ($Na_2Fe[Fe(CN)_6]$) and hard carbon anode were used as the active cathode and anode materials, respectively, and the capacity ratio of anode to cathode was approximately 1.3:1. Glass fibre was the separator with 100 μL of electrolyte added. The cell cycling procedure involved 3 × rate C/20 formation cycles followed by cycling at either rate C/3 or C/5. The cell cycling then concluded with 2 × rate C/20 diagnostic cycles.

When cycling 0.5 M $NaBPh_4$ in EC:DEC between voltage limits 1.5–3.6 V at rate C/3, the cell cycling performance was poor (Fig. 7). The C/3 cycles began with a capacity of *ca.* 140 mAh g^{-1}, but the capacity retention over the 300-cycle duration was low (43%, determined from 1st and last C/3 cycle). The Coulombic efficiencies (CEs) started low but increased during cycling and reached a maximum of 98.5% (Fig. 7b). The voltage *vs.* specific capacity plots for the 1st, 2nd and 305th (last) C/20 cycles have been compared and are shown in Fig. 7c. These plots show loss of the 2nd (lower) plateau from the 2nd to 305th discharge cycles, which corresponds to a phase transition between cubic and rhombohedral phases in the Prussian white cathode during cycling. Previous studies investigating capacity fade using Prussian white cathodes have revealed that most of the capacity is lost from this lower potential plateau.[29,30] The loss of the lower plateau in this work indicates sodium inventory loss,[29] mostly caused by parasitic oxidation of the electrolyte salt.

In an effort to improve the capacity retention when using 0.5 M $NaBPh_4$ in EC:DEC as the electrolyte, the upper cut-off voltage was reduced to either 3.4 V or 3.2 V. Cycling with voltage limits 1.5–3.4 V gave similar results to the cells using an upper cut-off voltage of 3.6 V, even when including 2 wt% $NaPF_6$ as an additive (Fig. 8). Although the inclusion of $NaPF_6$ as an additive introduces a source of fluorine to the electrolyte, it is known that during battery cycling $NaPF_6$ decomposes to form NaF.[31,32] The presence of NaF in the SEI has been reported to be a key interfacial component which enables long-term stable cycling.[20] Thus, the inclusion of a small quantity of $NaPF_6$ as an additive to the $NaBPh_4$-based electrolyte in this work was an attempt to improve interfacial stability, but as observed in Fig. 8 this did not improve the capacity retention or CEs under these cycling conditions (Fig. S14). However, by reducing the upper cut-off voltage to 3.2 V, greater cycling performance with an improved capacity retention was observed (62% after 100 cycles, Fig. 9).

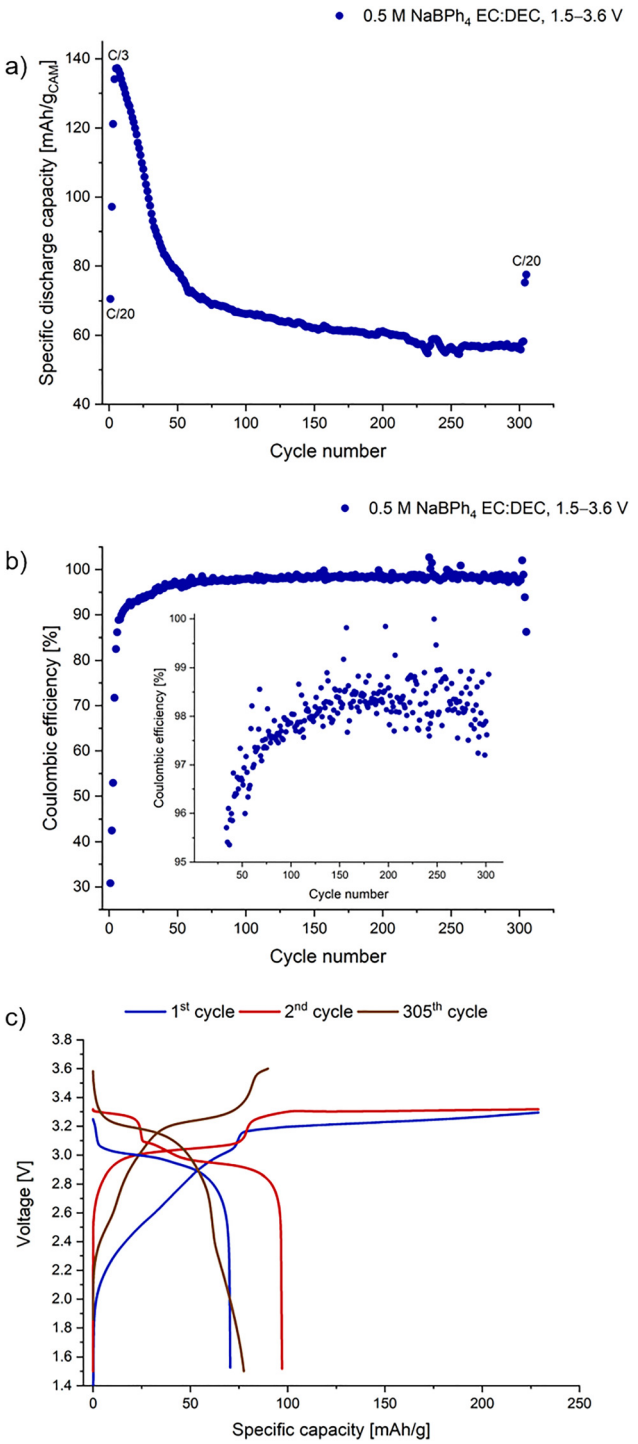

Fig. 7 (a) Specific discharge capacity *vs.* cycle number, (b) Coulombic efficiency *vs.* cycle number and (c) voltage *vs.* specific capacity for the 1st, 2nd and last (305th) C/20 cycles. Measured in coin cells using a Prussian white cathode and hard-carbon anode. The applied C-rates of C/20 and C/3 were calculated based on the expected capacity of 150 mAh g^{-1} of the cathode, using cell voltage limits of 1.5–3.6 V. Electrolyte is 0.5 M $NaBPh_4$ in EC:DEC (1:1 v/v), cycled at 21 °C.

To further improve the extended charge/discharge cycling, the cycling rate was decreased from rate C/3 to C/5. Coin cells were assembled and cycled using voltage limits of either

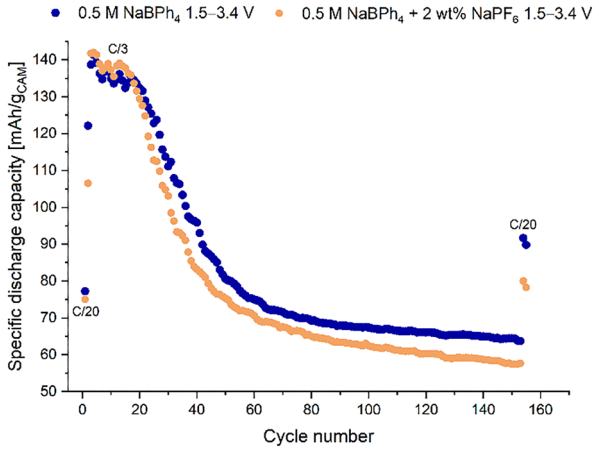

Fig. 8 Specific discharge capacity *vs.* cycle number using Prussian white cathode and hard-carbon anode. The applied C-rates of C/20 and C/3 were calculated based on the expected capacity of 150 mAh g^{-1} of the cathode, using cell voltage limits of 1.5–3.4 V. Electrolyte is 0.5 M $NaBPh_4$ (blue) and 0.5 M $NaBPh_4$ + 2 wt% $NaPF_6$ (orange) in EC:DEC (1:1 v/v), cycled at 21 °C. Measured in coin cells.

1.5–3.2 V or 1.5–3.0 V. While the initial capacity and capacity retention of the cells cycling between 1.5–3.2 V were comparable at either rate, cells cycling between 1.5–3.0 V were stable for the 200-cycles, albeit at lower capacity (75–70 mAh g^{-1}, Fig. 10a). Although the 1st cycle CE was low (33.5%), after 22 cycles the CE had reached 99.0%, where this was maintained (Fig. S16).

The voltage *vs.* specific capacity plots for the 1st, 2nd and last C/20 cycles have been compared for cells cycling up to both 3.2 V (Fig. 10b) and 3.0 V (Fig. 10c). As seen in Fig. 10c, the high stability of 0.5 M $NaBPh_4$ when cycled to 3.0 V can partly be explained by limiting the phase transition between the cubic and rhombohedral phases during cycling. Minimising this phase transition has previously been shown to enable stable cycling by limiting the amount of sodium inserted and extracted within the cathode.[33] However, the main contribution to the increased cell stability at 3.0 V in this work is attributed to limiting $NaBPh_4$ salt decomposition, which causes sodium inventory loss.

Thus, 0.5 M $NaBPh_4$ in EC:DEC can undergo stable long-term charge/discharge cycling, but it requires a low upper voltage limit. Although the lower energy obtained when cycling up to 3.0 V limits certain practical applications, the stable cycling may offer benefits for use in devices where the size and weight of the battery are not the primary concern, such as in home energy and grid-scale storage.

Cycling with $NaPF_6$ as the electrolyte salt was performed to compare to $NaBPh_4$. Long-term stable cycling was observed when using 1 M $NaPF_6$ in EC:DEC (1:1 v/v) in Prussian white *vs.* hard carbon cells, using voltage limits of 1.5–3.8 V (Fig. S17). This is on account of the wider ESW when using the fluorinated $NaPF_6$ salt.[34] Lastly, 1 M $NaPF_6$ was cycled using lower voltage limits of 1.5–3.2 V, at rate C/5. Stable cycling was again seen, but at lower capacities than when cycled up to 3.8 V (approximately 70 mAh g^{-1}, Fig. S19).

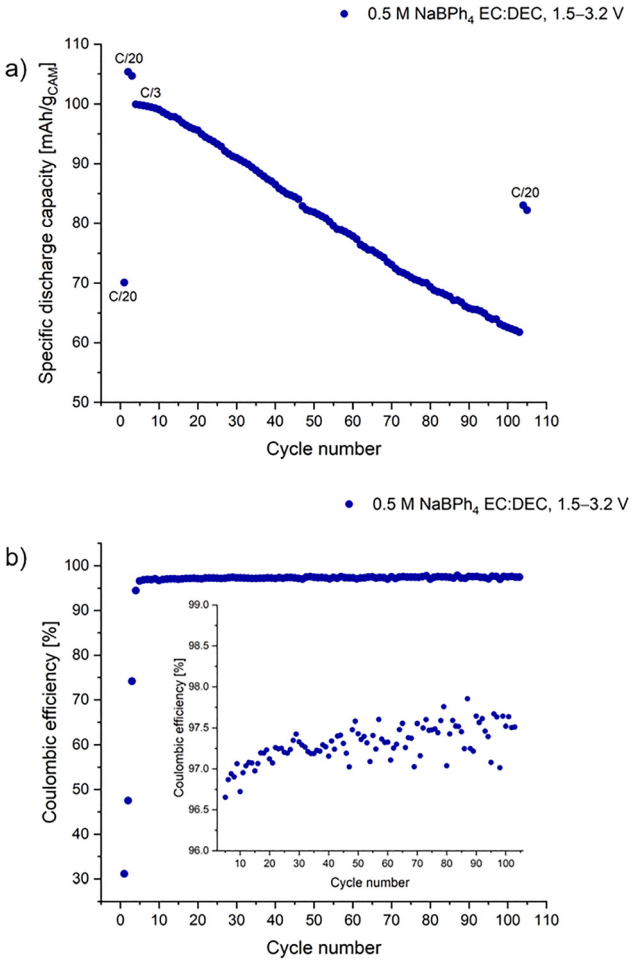

Fig. 9 (a) Specific discharge capacity *vs.* cycle number and (b) Coulombic efficiency *vs.* cycle number plots. Measured in coin cells using a Prussian white cathode and hard-carbon anode. The applied C-rates of C/20 and C/3 were calculated based on the expected capacity of 150 mAh g^{-1} of the cathode, using cell voltage limits of 1.5–3.2 V. Electrolyte is 0.5 M $NaBPh_4$ in EC:DEC (1:1 v/v), cycled at 21 °C.

To investigate the electrolyte degradation occurring in the cells using $NaBPh_4$ in EC:DEC, multinuclear solution-state NMR spectroscopy was performed. Coin cells that were cycled between voltage limits of either 1.5–3.2 V or 1.5–3.0 V at rate C/5 were opened in an inert atmosphere and the electrolyte was extracted from the glass-fibre separator using DMSO-d_6 as the NMR solvent. Previous reports investigating electrolyte degradation in LIBs using $LiPF_6$ in carbonate solvents with a layered transition metal oxide cathode, *e.g.* $LiNi_{0.8}Mn_{0.1}Co_{0.1}O_2$ (NMC811), have found O_2 is formed during cycling and reacts with ethylene carbonate (EC) to form CO_2, CO and H_2O.[35,36] The production of H_2O leads to secondary reactions and hydrolysis of the PF_6^- anion.[37] Fewer electrolyte degradation investigations have been performed for sodium-based electrolytes, but ring opening of EC to form 1,2-ethanediol and hydrolysis of the PF_6^- anion when using 1 M $NaPF_6$ in different carbonate solvents have been detected in a study using NMR spectroscopy.[8] Other studies have shown that replacing $NaPF_6$

with NaFSI as the electrolyte salt leads to fewer electrolyte decomposition products.[38,39]

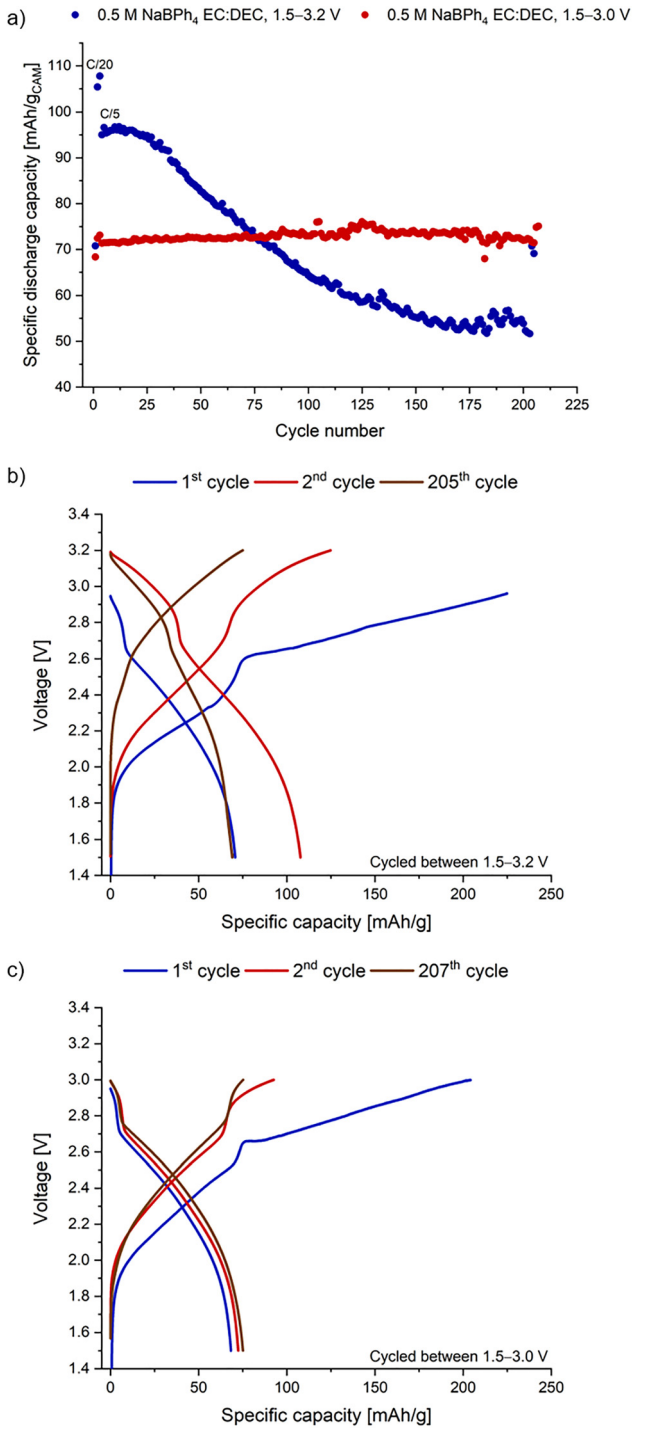

Fig. 10 (a) Specific discharge capacity *vs.* cycle number using cell voltage limits of 1.5–3.2 V (blue) or 1.5 V–3.0 (red). (b) Voltage *vs.* specific capacity for the 1st, 2nd and last (205th) C/20 cycles using cell voltage limits of 1.5–3.2 V. (c) Voltage *vs.* specific capacity for the 1st, 2nd and last (207th) C/20 cycle using cell voltage limits of 1.5–3.0 V. Measured in coin cells using a Prussian white cathode and hard-carbon anode. The applied C-rates of C/20 and C/5 were calculated based on the expected capacity of 150 mAh g^{-1} of the cathode. Electrolyte is 0.5 M $NaBPh_4$ in EC:DEC (1:1 v/v). Cells cycled at 21 °C.

The ^{1}H NMR spectrum of the post-cycled electrolyte from coin cells cycled between voltage limits of 1.5–3.0 V at rate C/5 showed a loss of approximately 50% diethyl carbonate (DEC) solvent compared to the pristine electrolyte (Fig. 11a). This was determined by integrating the DEC solvent signals [δ_H = 4.10 ppm (CH_2) and 1.20 ppm (CH_3)] against the EC signal (δ_H = 4.48 ppm). This assumes that the amount of EC remains constant during cycling, which may not be accurate due to degradation (for example, during SEI formation). The high loss of DEC is also likely explained by evaporation of the solvent when preparing the NMR sample. A strong intensity singlet at δ_H = 3.31 ppm is observed in the ^{1}H NMR spectrum and is assigned to water. Water may have formed from the decomposition of the carbonate solvent during cycling, but as water is

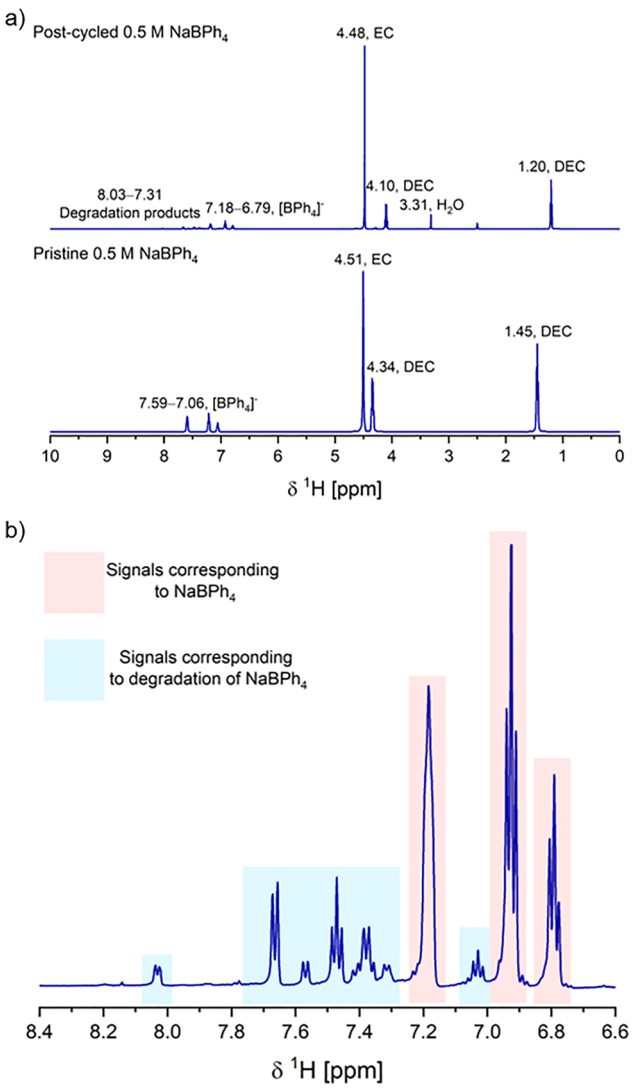

Fig. 11 (a) Top: ^{1}H NMR (500 MHz, $(CD_3)_2SO$, 295 K) spectrum of post-cycled 0.5 M $NaBPh_4$ in EC:DEC solvent after 200 cycles between voltage limits 1.5–3.0 V. Bottom: ^{1}H NMR (500 MHz, $CDCl_3$, 295 K) spectrum of pristine 0.5 M $NaBPh_4$ in EC:DEC. (b) ^{1}H NMR (500 MHz, $(CD_3)_2SO$, 295 K) spectrum of post-cycled 0.5 M $NaBPh_4$ in EC:DEC solvent after 200 cycles between voltage limits 1.5–3.0 V, focussed on the aromatic region.

also present in the DMSO-d_6 solvent it is not possible to quantify this accurately.

A low intensity singlet at δ_H = 4.28 ppm is observed in the ^{1}H NMR spectrum of the post-cycled electrolyte, which when studying electrolyte degradation in LIBs has been assigned to lithium ethylene dicarbonate (LEDC), which forms from the reduction of EC.[35,36] Thus, the signal at δ_H = 4.28 ppm observed in this work may arise from sodium ethylene dicarbonate (NEDC, $NaO_2CO–C_2H_4–OCO_2Na$, Scheme 1a). NEDC has previously been detected in XPS studies on post-cycled hard carbon when using either 1 M $NaPF_6$ or 1 M NaTFSI in ethylene carbonate: dimethyl carbonate (EC:DMC) solvent as the electrolyte and was shown to be a crucial SEI component.[20] A very low intensity singlet at δ_H = 8.14 ppm was also observed and has previously been assigned to formic acid, resulting from the decomposition of DMC solvent.[35] While the signal at δ_H = 8.14 ppm in this work is tentatively assigned to formic acid, other decomposition products from DEC were not clearly observed in the ^{1}H NMR spectrum, such as ethanol, methanol, ethyl formate or methyl acetate.[43] The findings of the limited degradation of DEC solvent is in agreement with a previous report finding that linear carbonates exhibit a decreasing rate of degradation as the aliphatic chain length increases, of the order DMC > ethyl methyl carbonate (EMC) > DEC.[8]

The pristine electrolyte of 0.5 M $NaBPh_4$ in EC:DEC solvent shows three aromatic signals in the ^{1}H NMR spectrum; δ_H = 7.59 ppm, δ_H = 7.22 ppm and δ_H = 7.06 ppm, when using $CDCl_3$ as the NMR solvent. These signals correspond to the aromatic rings of the $[BPh_4]^-$ anion. The post-cycled electrolyte of cells cycled up to 3.0 V showed these three signals in the ^{1}H NMR spectrum (δ_H = 7.18 ppm, 6.93 ppm and 6.79 ppm in DMSO-d_6 solvent), corresponding to the $[BPh_4]^-$ anion, but also showed additional aromatic signals. These additional signals are from decomposition of the $NaBPh_4$ salt (Fig. 11b).

Datta and colleagues have investigated the electrochemical oxidation of the $[BPh_4]^-$ anion using CV and coulometry in a series of different solvents, finding that the oxidation mechanism is dependent on solvent polarity (Scheme 1b).[41] In low dielectric solvents, such as dichloromethane, the $[BPh_4]^-$ anion undergoes a one-electron oxidation that is not fully reversible. The mechanism in higher dielectric solvents was found to be more complicated due to secondary chemical reactions occurring but coulometry experiments revealed a two-electron process. Triphenylborane (BPh_3, which may be solvated) and biphenyl (Ph_2), which is formed from the radical coupling reaction of two phenyl radicals, were suggested as oxidation products. Coulometry experiments found in solvents other than dichloromethane, disproportionation of S–BPh_3 (S = solvent) takes place, regenerating $[BPh_4]^-$ and forming a new species, S–BPh_2^+.[41] These findings are in agreement with earlier work from Geske, who studied the oxidation of $NaBPh_4$ in acetonitrile solvent.[42] A two-electron irreversible oxidation mechanism was proposed, forming BPh_2^+ and biphenyl. BPh_2^+ then underwent secondary chemical reactions to form triphenylborane and benzene amongst other products.[42]

In the ^{1}H NMR spectrum of the post-cycled electrolyte in our work, there is evidence of biphenyl, with the doublet at δ_H = 7.66 ppm ($^3J_{HH}$ = 7.5 Hz) and triplet at 7.47 ppm ($^3J_{HH}$ = 7.5 Hz) matching the signals from a separately prepared sample of pristine biphenyl in DMSO-d_6 solvent (Fig. S34). In addition, the ^{1}H NMR spectrum showed evidence of triphenylborane, with the doublet at δ_H = 7.31 ppm ($^3J_{HH}$ = 7.4 Hz) and triplet at 7.03 ppm ($^3J_{HH}$ = 7.4 Hz) matching the signals from a separately prepared sample of pristine triphenylborane in DMSO-d_6 solvent (Fig. S35). However, there was no clear evidence of triphenylborane in the ^{11}B NMR spectrum of the post-cycled electrolyte, with only the signal at −6.7 ppm (corresponding to the BPh_4^- anion) being observed (Fig. 12). Integrating the signals corresponding to $NaBPh_4$: signals corresponding to decomposition products gave a ratio of 1:0.35. We do not rule out the formation of other decomposition products in addition to biphenyl and triphenylborane.

Similar findings were found in the ^{1}H NMR spectrum of post-cycled electrolyte from cells cycled up to 3.2 V at rate C/5 (Fig. S32). Interestingly, the signals which were assigned to

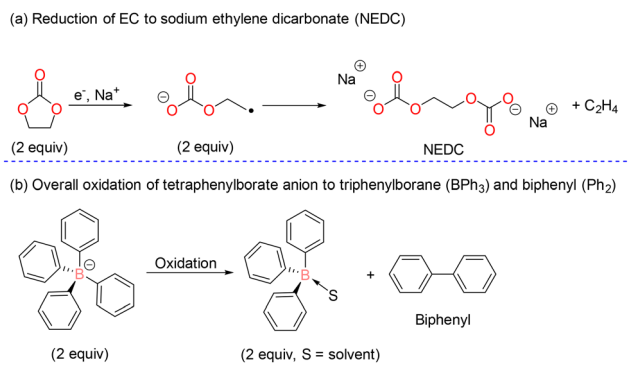

Scheme 1 (a) Formation of sodium ethylene dicarbonate (NEDC) from the reduction of ethylene carbonate (EC), adapted from the formation of lithium ethylene dicarbonate (LEDC).[35,40] (b) Overall oxidation reaction of the tetraphenylborate anion to form (solvated) triphenylborane and biphenyl, hypothesised to occur in this work.[41,42]

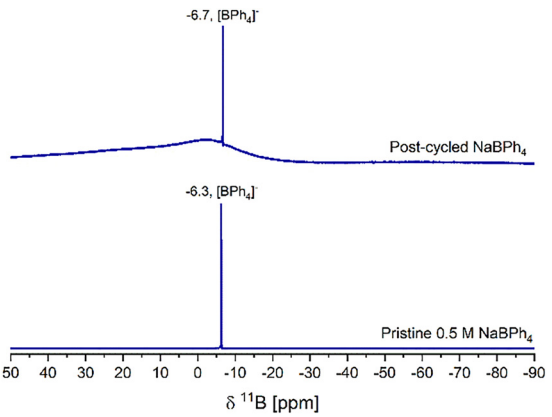

Fig. 12 Top: ^{11}B NMR (160 MHz, $(CD_3)_2SO$, 295 K) spectrum of post-cycled 0.5 M $NaBPh_4$ in EC:DEC solvent after 200 cycles between voltage limits 1.5–3.0 V. Bottom: ^{11}B NMR (160 MHz, $CDCl_3$, 295 K) spectrum of pristine 0.5 M $NaBPh_4$ in EC:DEC.

biphenyl have grown in intensity for the cells cycled up to 3.2 V. Thus, suggesting more degradation of the $NaBPh_4$ salt takes place at higher voltages. The very low intensity signal at $\delta_B = -6.7$ ppm in the ^{11}B NMR spectrum, corresponding to $NaBPh_4$, supports greater salt degradation in the 1.5–3.2 V cells (Fig. S33). No other signals were observed in the ^{11}B NMR spectrum. Moreover, when preparing the NMR solutions, the colour of the post-cycled electrolyte for the 1.5–3.2 V cells was dark yellow in colour, compared to the colourless appearance of the post-cycled electrolyte from the 1.5–3.0 V cells (Fig. S36).

The electrochemical oxidation of the $NaBPh_4$ salt may explain the poor capacity retention observed during battery cycling at higher voltages, due to sodium inventory loss. The electrochemical breakdown of the $[BPh_4]^-$ anion in this work contrasts previous reports using $NaBPh_4$ in DME as the electrolyte in copper *vs.* sodium and hard carbon *vs.* sodium half-cells, where XPS analysis found minimal/no decomposition of $NaBPh_4$.[24,25] Thus, while 0.5 M $NaBPh_4$ in EC:DEC electrolyte can undergo stable charge/discharge cycling in sodium-ion full-cells, low upper voltages are required, with this electrolyte best suited for low voltage cathode materials. Future research efforts should look to increase the oxidative stability of this electrolyte, for example through solvent or additive design,[44–46] which would maximise the full potential of using $NaBPh_4$ as a fluorine-free electrolyte salt for SIBs.

Conclusions

In conclusion, sodium tetraphenylborate ($NaBPh_4$) has been used as a non-fluorinated electrolyte salt for SIBs, improving the safety of the battery by preventing toxic HF formation. $NaBPh_4$ possesses good thermal stability and a high tolerance to atmospheric air, affording safe and convenient handling, transport and storage. The bulk conductivities of $NaBPh_4$ in EC:DEC solvent (1:1 v/v) at different concentrations were measured, where 0.5 M $NaBPh_4$ gave the highest conductivity. By measuring the corresponding viscosities of the electrolyte solutions, this was explained as being a balance between increasing the number of conductive charge carriers in solution *versus* the corresponding large increase in the viscosity beyond 0.5 M concentration.

0.5 M $NaBPh_4$ in EC:DEC was cycled in sodium-ion coin cells containing a Prussian white cathode and hard carbon anode. When cycled using an upper cut-off voltage of 3.6 V, the capacity retention was poor. By lowering the upper cut-off voltage, the capacity retention improved and long-term stable cycling was observed when using voltage limits 1.5–3.0 V, but with lower capacities. Solution-state NMR spectroscopy was performed on the post-cycled electrolyte and found degradation of the $NaBPh_4$ salt, with triphenylborane and biphenyl hypothesised as likely decomposition products. The electrochemical oxidation of $NaBPh_4$ during cycling can in part explain the poor capacity retention when cycled at higher voltages. Therefore, these results have shown 0.5 M $NaBPh_4$ in EC:DEC electrolyte can undergo stable long-term charge/discharge cycling, but it requires low voltages (3.0 V). Future research should aim to improve the oxidative stability of this electrolyte to enable its widespread uptake for application in sodium-ion batteries.

Experimental

Sodium tetraphenylborate ($NaBPh_4$) was purchased from Sigma Aldrich (U.K.). The electrolyte solutions of sodium tetraphenylborate ($NaBPh_4$) in ethylene carbonate: diethyl carbonate (EC:DEC 1:1 v/v) solvent were prepared by dissolving the required amount of salt in the binary solvent mixture. The $NaBPh_4$ salt has good solubility in EC:DEC solvent, however, for the higher electrolyte concentrations it took longer for the salt to fully dissolve (approximately a few hours). To minimise water content, $NaBPh_4$ was dried at 110 °C for 18 hours under vacuum (1×10^{-2} mbar). From Karl–Fischer titration measurements, the water concentration in the $NaBPh_4$ in EC:DEC electrolyte solutions were 6 ppm (0.1 M), 26 ppm (0.25 M), 55 ppm (0.5 M), 91 ppm (1 M) and 100 ppm (1.5 M).

Ethylene carbonate:diethyl carbonate (EC:DEC 1:1 v/v) solvent was prepared by weighing a known amount of EC and translating this to a volume using the density 1.321 g mL^{-1}. The equal volume of DEC was added; gentle heating to 50 °C was required to fully dissolve EC. The 1:1 by volume ratio was confirmed by integrating the EC and DEC signals in the ^1H NMR spectrum. The prepared solvent was degassed using freeze–pump–thaw degas technique and dried over 4 Å activated molecular sieves to *ca.* 10 ppm water (determined by Karl–Fischer titration).

Prussian white, $Na_2Fe[Fe(CN)_6]$, was synthesised using an adapted two-step method.[47,48] Prussian blue (PB) was synthesised from $Na_4Fe(CN)_6{\cdot}10H_2O$ and ascorbic acid in 0.1 M HCl, gradually heated to 80 °C and stirred for 4 hours to form high-quality crystals. The product was centrifuged and washed repeatedly with ethanol–water (1:1 v/v). Prussian white was obtained by reducing the PB suspension with stoichiometric $NaBH_4$ for 30 minutes under ambient conditions. The resulting Prussian white was washed with ethanol and thoroughly dried under heat–vacuum (170 °C, 2×10^{-2} mbar, 20 hours) to remove residual moisture and minimise oxidation. Resulting rhombohedral Prussian white powder was stored in an argon filled glove box to avoid oxidation. The electrodes were prepared by mixing Prussian white powder, Super-P® carbon black, carboxymethylcellulose (CMC, MW = 90 000) and styrene-butadiene rubber (SBR) to form a slurry. The ratios were respectively 80 : 10 : 3 : 7 wt%. Deionised water was used as solvent. The components were mixed in Thinky mixer (THINKY ARE-250) in steps, starting with dissolving CMC in water, then adding carbon black, then active material and finally SBR binder. The slurry was coated on 15 μm aluminium foil (battery-grade MTI) using an automatic film coater (MSK-AFA-II-VC-FH-MTI) and doctor blade and subsequently dried at 170 °C at $\times 10^{-3}$ mbar for 24 hours before being transferred to the glovebox for use in a cell. The negative electrode was prepared in similar way using a commercially available hard

carbon from Batri Ltd (Wales, U.K.). The ratios were 80 : 10 : 10 wt% for hard carbon, Super P and CMC binder, respectively. The electrodes were dried at 100 °C at $\times 10^{-2}$ mbar for 24 hours.

Coin cells (2032 from Cambridge energy solutions) were prepared in an argon glovebox (MBraun, $O_2 < 5$ ppm, $H_2O <$ 1 ppm). For Na-ion coin cells, a Prussian white cathode of area 1.33 cm^2 was assembled with a geometrically over-sized hard-carbon anode (1.54 cm^2). The n : p ratio was approximately 1.3:1. Glass fibre was used as the separator, which was dried at 80 °C under vacuum for 48 hours prior to using; 100 μL of electrolyte was added to the separator.

Thermogravimetric analysis (TGA) data was recorded with a TA Instruments SDT Q600 thermogravimetric analyser. A few milligrams of sample (sodium tetraphenylborate) were taken out of the argon filled glovebox and immediately transferred to the TGA heating chamber to minimise air exposure. All the measurements were performed from 25 °C to 600 °C with a heating rate of 10 °C min^{-1} and under an argon flow.

Solution ionic conductivity measurements were performed using an in-house designed two-electrode platinum cell (see Fig. S2). 2 mL of each electrolyte was filled into the cell and the rubber septum was sealed with parafilm to prevent air/moisture exposure. Impedance spectra were measured using an Invium potentiostat with an applied voltage amplitude of 25 mV and frequencies between 10 kHz and 0.1 Hz. The temperature was kept constant by submerging the electrolyte solution in a silicon oil bath at 25 °C. Impedance spectra were fitted using the circuit R + Q. The solution conductivity was found by taking the reciprocal of the R component, multiplied by the cell constant (10.2 ± 0.3 cm^{-1}, see SI).

Viscosity measurements were performed using a TA Instruments HR30 rheometer fitted with a 60 mm diameter hard anodised aluminium parallel plate geometry at a geometry gap of 400 μm. Temperature control was achieved using a lower Peltier plate geometry and evaporation was controlled using a solvent trap. Preliminary shear rate sweeps were performed to confirm that the sample behaved as Newtonain fluids (and hence could be characterised using a single, constant, viscosity parameter, μ).

The studied electrolytes' electrochemical stability window (ESW) was determined using cyclic voltammetry (CV). The electrolyte solutions in EC:DEC (1:1 v/v) solvent were tested in three-electrode cells (in house designed) using either glassy carbon or aluminium as the working electrode (WE). Platinum and sodium were used as the counter electrode and pseudo reference electrode, respectively. The three-electrode cell is a ''beaker style'' cell that uses an excess of electrolyte (2 mL) and does not use a separator. Each CV experiment comprised of five consecutive CV scans, at either 10 mV s^{-1} or 5 mV s^{-1}, for the glassy carbon and aluminium working electrode, respectively.

Author contributions

DMCO performed the NMR, bulk conductivity, CV and cell cycling experiments (analysing the corresponding data), wrote the manuscript and oversaw the project. JMC assisted with the analysis of the electrochemistry results and recorded SEM images of the aluminium foils. KGP performed the DOSY NMR experiments. DJC acquired and analysed the viscometric data. MWO, SJ and BdB provided the active materials and electrodes for sodium-ion cycling. SM provided materials, laboratory infrastructure and resources and oversaw the direction of the project. All authors have read and approved the manuscript.

Conflicts of interest

There are no conflicts to declare.

Data availability

The data supporting this article have been included as part of the supplementary information (SI). Supplementary information: electrochemistry and NMR figures. See DOI: https://doi.org/10.1039/d5ya00361j.

Acknowledgements

SM acknowledges support from the Royal Society through an Industry Fellowship (IF\R2\23200112). DMCO and SM also acknowledge funding from the Faraday Institution through the Industry SPRINT programme (grant number FIRG074) and Batri Ltd for supply of hard carbon.

Notes and references

1 C. P. Grey and D. S. Hall, *Nat. Commun.*, 2020, **11**, 6279.
2 T. Kim, W. Song, D.-Y. Son, L. K. Ono and Y. Qi, *J. Mater. Chem. A*, 2019, **7**, 2942–2964.
3 A. Manthiram, *ACS Cent. Sci.*, 2017, **3**, 1063–1069.
4 S. Chu, S. Guo and H. Zhou, *Chem. Soc. Rev.*, 2021, **50**, 13189–13235.
5 A. Ponrouch, E. Marchante, M. Courty, J.-M. Tarascon and M. R. Palacín, *Energy Environ. Sci.*, 2012, **5**, 8572–8583.
6 D. M. C. Ould, S. Oswald, H. E. Smith, C. A. O'Keefe, T. Song, E. Kendrick, D. S. Wright and C. P. Grey, *Chem. Commun.*, 2025, **61**, 8516–8519.
7 P. J. Buitrago Botero, A. W. Ells, A. Svirinovsky-Arbeli, M. Juelsholt and L. E. Marbella, *J. Am. Chem. Soc.*, 2025, **147**, 9159–9174.
8 P. Barnes, K. Smith, R. Parrish, C. Jones, P. Skinner, E. Storch, Q. White, C. Deng, D. Karsann, M. L. Lau, J. J. Dumais, E. J. Dufek and H. Xiong, *J. Power Sources*, 2020, **447**, 227363.
9 F. Larsson, P. Andersson, P. Blomqvist and B.-E. Mellander, *Sci. Rep.*, 2017, **7**, 10018.
10 L. Kong, Y. Li and W. Feng, *Electrochem. Energy Rev.*, 2021, **4**, 633–679.
11 A. Ponrouch, D. Monti, A. Boschin, B. Steen, P. Johansson and M. R. Palacín, *J. Mater. Chem. A*, 2015, **3**, 22–42.

12 L. G. Chagas, S. Jeong, I. Hasa and S. Passerini, *ACS Appl. Mater. Interfaces*, 2019, **11**, 22278–22289.
13 J. Serra Moreno, G. Maresca, S. Panero, B. Scrosati and G. B. Appetecchi, *Electrochem. Commun.*, 2014, **43**, 1–4.
14 S. Di Muzio, A. Paolone and S. Brutti, *J. Electrochem. Soc.*, 2021, **168**, 100514.
15 L. O. S. Colbin, C. A. Hall, A. S. Etman, A. Buckel, L. Nyholm and R. Younesi, *Energy Adv.*, 2024, **3**, 143–148.
16 L. Huang, Q. Qiu, M. Yang, H. Li, J. Zhu, W. Zhang, S. Wang, L. Xia and P. Müller-Buschbaum, *ACS Appl. Mater. Interfaces*, 2024, **16**, 46392–46400.
17 B. Vinay, Y. Nikodimos, T. Agnihotri, S. A. Ahmed, T. Mezgebe Hagos, R. Hasan, E. Balaji Tamilarasan, W.-N. Su and B. J. Hwang, *Energy Environ. Sci.*, 2025, **18**, 7326–7372.
18 G. Hernández, R. Mogensen, R. Younesi and J. Mindemark, *Batteries Supercaps*, 2022, **5**, e202100373.
19 D. M. C. Ould, S. Menkin, H. E. Smith, V. Riesgo-Gonzalez, E. Jónsson, C. A. O'Keefe, F. Coowar, J. Barker, A. D. Bond, C. P. Grey and D. S. Wright, *Angew. Chem., Int. Ed.*, 2022, **61**, e202202133.
20 J. Fondard, E. Irisarri, C. Courrèges, M. R. Palacin, A. Ponrouch and R. Dedryvère, *J. Electrochem. Soc.*, 2020, **167**, 070526.
21 R. Mogensen, S. Colbin, A. S. Menon, E. Björklund and R. Younesi, *ACS Appl. Energy Mater.*, 2020, **3**, 4974–4982.
22 R. Mogensen, A. Buckel, S. Colbin and R. Younesi, *Chem. Mater.*, 2021, **33**, 1130–1139.
23 L. O. S. Colbin, R. Mogensen, A. Buckel, Y.-L. Wang, A. J. Naylor, J. Kullgren and R. Younesi, *Adv. Mater. Interfaces*, 2021, **8**, 2101135.
24 K. Doi, Y. Yamada, M. Okoshi, J. Ono, C.-P. Chou, H. Nakai and A. Yamada, *Angew. Chem., Int. Ed.*, 2019, **58**, 8024–8028.
25 Y. Morikawa, Y. Yamada, K. Doi, S.-I. Nishimura and A. Yamada, *Electrochemistry*, 2020, **88**, 151–156.
26 C. Chu, L. Zhou, Y. Cheng, X. Wang, L. Chang, P. Nie, C. Wang and L. Wang, *Chem. Eng. J.*, 2024, **482**, 148915.
27 K. Qian, Z. Yu, Y. Liu, D. J. Gosztola, R. E. Winans, L. Cheng and T. Li, *J. Energy Chem.*, 2022, **70**, 340–346.
28 K. N. Ninan and C. G. R. Nair, *Thermochim. Acta*, 1976, **15**, 345–353; K. N. Ninan and C. G. R. Nair, *Thermochim. Acta*, 1976, **15**, 345–353.
29 I. Nielsen, C. A. Hall, A.-M. Mattsson, R. Younesi, A. Buckel and W. R. Brant, *J. Mater. Chem. A*, 2024, **12**, 17413–17421.
30 W. R. Brant, R. Mogensen, S. Colbin, D. O. Ojwang, S. Schmid, L. Häggström, T. Ericsson, A. Jaworski, A. J. Pell and R. Younesi, *Chem. Mater.*, 2019, **31**, 7203–7211.
31 Y. Steinberg, E. Sebti, I. B. Moroz, A. Zohar, D. Jardon-Alvarez, T. Bendikov, A. Maity, R. Carmieli, R. J. Clément and M. Leskes, *J. Am. Chem. Soc.*, 2024, **146**, 24476–24492.
32 K. Hankins, M. H. Putra, J. Wagner-Henke, A. Groß and U. Krewer, *Adv. Energy Mater.*, 2024, 2401153.
33 L. Shen, Y. Jiang, Y. Liu, J. Ma, T. Sun and N. Zhu, *Chem. Eng. J.*, 2020, **388**, 124228.
34 D. M. C. Ould, J. M. Courtney, D. J. Morgan, D. J. Curtis, M. W. Orzech, S. Kiani, B. de Boode, C. P. Grey, D. S. Wright and S. Margadonna, *EES Batteries*, 2026, **2**, 475–489.
35 B. L. D. Rinkel, D. S. Hall, I. Temprano and C. P. Grey, *J. Am. Chem. Soc.*, 2020, **142**, 15058–15074.
36 B. L. D. Rinkel, J. Padmanabhan Vivek, N. Garcia-Araez and C. P. Grey, *Energy Environ. Sci.*, 2022, **15**, 3416–3438.
37 S. Wiemers-Meyer, M. Winter and S. Nowak, *Phys. Chem. Chem. Phys.*, 2016, **18**, 26595–26601.
38 W. Black, Z. Ye, H. Hijazi, S. Azam, M. Garayt and M. Metzger, *J. Electrochem. Soc.*, 2025, **172**, 070525.
39 Z. Ye, H. Hijazi, W. Black, S. Azam, J. R. Dahn and M. Metzger, *J. Electrochem. Soc.*, 2024, **171**, 040522.
40 Y. Wang, S. Nakamura, M. Ue and P. B. Balbuena, *J. Am. Chem. Soc.*, 2001, **123**, 11708–11718.
41 P. K. Pal, S. Chowdhury, M. G. B. Drew and D. Datta, *New J. Chem.*, 2002, **26**, 367–371.
42 D. H. Geske, *J. Phys. Chem.*, 1959, **63**, 1062–1070.
43 B. Dong, L. Wang, L. Hu, J. Fang and Z. Wang, *Proc. Combust. Inst.*, 2024, **40**, 105479.
44 J. Ning, M. Zhou, Y. Zhang, T. Wang, M. Chen, Q. Cu, K. Wang, W. Wang, H. Li and K. Jiang, *EcoEnergy*, 2025, **3**, e70006.
45 M. Ma, R. Huang, M. Ling, Y.-S. Hu and H. Pan, *Interdiscip. Mater.*, 2023, **2**, 833–854.
46 Q. Cao, D. Fu, X. He, Y. Huang, N. Yao, C. Song, H. Song and C. Wang, *Nano-Micro Lett.*, 2026, **18**, 243.
47 A. Willow, M. Orzech, S. Kiani, N. Reynolds, M. Houchell, O. Omisore, Z. Tehrani and S. Margadonna, *Batteries*, 2025, **11**, 97.
48 C. Q. X. Lim and Z.-K. Tan, *ACS Appl. Energy Mater.*, 2021, **4**, 6214–6220.